Journal of Applied Physics

RESEARCH ARTICLE | APRIL 01 2026

Influence of cadmium ion doping on luminescence of $CsPbBr_3$ single crystals

V. Shvets ; A. Pushak ; O. Antonyak ; R. Gamernyk ; A. Kotlov; Y. Smortsova ; V. Salapak ; A. Zelinskiy ; V. Stakhura ; O. Bovgyra ; T. Demkiv ; A. Voloshinovskii

J. Appl. Phys. 139, 135101 (2026)
https://doi.org/10.1063/5.0306690

Journal of Applied Physics ARTICLE pubs.aip.org/aip/jap

Influence of cadmium ion doping on luminescence of $CsPbBr_3$ single crystals

Cite as: J. Appl. Phys. **139**, 135101 (2026); doi: 10.1063/5.0306690
Submitted: 11 October 2025 · Accepted: 3 March 2026 ·
Published Online: 1 April 2026

V. Shvets,[1] A. Pushak,[1] O. Antonyak,[1] R. Gamernyk,[1] A. Kotlov,[2] Y. Smortsova,[2] V. Salapak,[3] A. Zelinskiy,[1] V. Stakhura,[1] O. Bovgyra,[1] T. Demkiv,[1,a)] and A. Voloshinovskii[1]

AFFILIATIONS

[1]Ivan Franko National University of Lviv, 8 Kyryla i Mefodiya str., Lviv 79005, Ukraine
[2]Deutsch's Elektronen-Synchrotron DESY, Notkestrasse 85, Hamburg 22607, Germany
[3]The National Forestry University of Ukraine, Lviv 79057, Ukraine

[a)]**Author to whom correspondence should be addressed:** taras.demkiv@lnu.edu.ua

ABSTRACT

The effect of impurity doping with cadmium ions on the luminescent properties of $CsPbBr_3$ perovskite single crystals has been investigated. The luminescence spectra of pure and Cd-activated $CsPbBr_3$ crystals, obtained upon excitation with synchrotron radiation, reveal characteristic excitonic bands, which are interpreted as the emission of free and bound excitons in the vicinity of the crystal absorption edge, a broadband luminescence at 556.3 nm, and additional luminescence bands at 920 nm. The introduction of Cd is shown to result in an increase in the intensity of the excitonic luminescence, the emergence of supplementary emission bands due to the scattering of excitons on quasilocal lattice vibrations, and a shift of the near-edge luminescence bands toward the high-energy region. Cadmium doping is proposed to improve the tolerance factor of the perovskite structure, reduce the concentration of bromine vacancies, and increase the formation energy of anionic vacancies in Cd–Br pairs, thereby limiting halogen diffusion. These modifications lead to a reduction in non-radiative relaxation channels and enhance the efficiency of near-edge luminescence by a factor of 4. The luminescence band at 920 nm is attributed to the emission of radiation-induced defects. The results obtained highlight the potential of $CsPbBr_3$–Cd single crystals for the development of fast scintillators with improved light output.

I. INTRODUCTION

Fully inorganic lead halide perovskites $CsPbX_3$ (where X = Cl, Br, and I) have attracted significant attention due to their high photoluminescence quantum yield, narrow photoluminescence lines, high density, large resistivity, and carrier mobility–lifetime product ($\sim 10^{-3}$ cm^2/V), as well as a bandgap that can be tuned over a wide range by varying the halide X in the $CsPbX_3$ matrix.[1–3] These properties make $CsPbX_3$ perovskites promising candidates for a variety of optoelectronic applications, including light-emitting diodes,[4–6] solar cells,[7–10] photodetectors,[10,11] and current and luminescent detectors of ionizing radiation.[12–15]

In addition, perovskites have continuously attracted attention as scintillators. In Refs. 16 and 17, the prospects of using $CsPbBr_3$ and $CsPbCl_3$ crystals as cryogenic scintillators with short decay times were demonstrated. For example, at 7 K, a $CsPbBr_3$ crystal shows a light yield of about 50 000 ph/MeV under excitation with 12 keV x rays and a decay constant of ~1 ns,[18] while $CsPbCl_3$ exhibits a light yield of about 19 000 ph/MeV under excitation with 14 keV x rays at 10 K and the fastest decay constant of ~0.1 ns.[16]

A significant contribution is the work of Dorenbos,[19] in which he demonstrates that the integral light yield of $CsPbBr_3$ crystals under x-ray excitation at 10 K amounts to 34 000 photons/MeV, while the fast component alone reaches only 10 500 photons/MeV. Considering the multiple attempts to evaluate the scintillation efficiency of lead halide crystals, the scintillation yield of these crystals remains a subject of ongoing investigation and refinement.

If isovalent substitution of Pb^{2+} with divalent metal cations results in improved luminescence performance, activation with lanthanide ions (La) leads to a substantial reduction in the light yield.[20] A 17-fold increase in luminescence intensity was also reported upon activation with the monovalent Li^+ cation for $Cs_{1-x}Li_xPbCl_3$ single

crystals at x = 0.03%.[21] These examples indicate that perovskites exhibit defect tolerance, which opens new opportunities for the engineering of these crystals.

We identify a pathway to enhance the performance of perovskite halide scintillators. Insights for this approach were inspired by strategies used to improve the luminescence efficiency of nanoparticles. Activation of these nanoparticles with metals such as Cd, Mg, Ni, and Cu resulted in a significant increase in photoluminescence intensity.[18] For instance, doping $CsPbBr_3$ nanoparticles with magnesium led to an increase in the photoluminescence quantum yield from ∼51% to ∼100%.[22] Similarly, $CsPbBr_3$ nanocrystals doped with a substantial amount of Ce^{3+} ions (up to 2.88 at. %) exhibited a twofold increase in quantum yield (up to 89%) compared to undoped $CsPbBr_3$ nanocrystals.[23] Doping with various monovalent, divalent, and heterovalent metal ions (Ca^{2+}, Sr^{2+}, Na^{+}, Ce^{3+}, Sb^{3+}) also resulted in an enhancement of the quantum yield of perovskite nanocrystals.[24–27]

Among these modifications, the most pronounced effects were observed in $CsPbCl_3$ nanoparticles, where doping with Cd^{2+} and Mg^{2+} cations increased the luminescence quantum yield from ∼1% to 100%.[27] The improvement in luminescence efficiency is attributed to the refinement of the crystal matrix, including enhanced short-range order, effective surface passivation of nanoparticles, and a reduction in the concentration of point defects, particularly Cl^{-} vacancies. The conclusion regarding matrix ordering during the activation of perovskites is supported by the analyses of their luminescent characteristics, as well as independent structural and spectroscopic studies (EXAFS,[27] XPS[22]) and quantum-mechanical modeling of defect energy levels,[26,18] which indicate a shift of defect levels toward reduced participation in non-radiative processes. However, perovskite nanoparticles often suffer from low stability under typical conditions, and the presence of surface defects facilitates non-radiative recombination, thereby deteriorating their optical properties.[28]

We aim to implement the strategy of enhancing the luminescence quantum yield of nanoparticles through metal doping in $CsPbBr_3$ single crystals. Bulk perovskite scintillators exhibit significantly higher stability and possess intense picosecond excitonic luminescence in the low-temperature region, indicating their potential for applications as cryogenic scintillators and detectors of high-energy radiation.[29] Promising results have already been achieved for $CsPbCl_3$ crystals,[17] where a substantial increase in luminescence intensity was obtained upon doping with Cd ions.

This work analyzes the spectral and temporal parameters of near-edge luminescence of $CsPbBr_3$ single crystals activated with Cd^{2+} ions and excited by synchrotron radiation quanta. Such studies are important not only for clarifying the mechanisms of enhancement of near-edge luminescence intensity in single crystals but also for identifying directions in the development of new scintillators with high light yield and short luminescence decay times.

II. EXPERIMENTAL SECTION

$CsPbBr_3$ single crystals were grown by the Stockbarger method from CsBr and $PbBr_2$ precursors mixed in a stoichiometric ratio. CsBr salt (99.999% purity) and $PbBr_2$ salt (98% purity) were used; the latter was additionally purified by several stages of zone refining. For crystal activation, $CdBr_2$ salt (99.99% purity) was added to the charge in excess with respect to the stoichiometric composition. The nominal $CdBr_2$ concentrations (0.5, 1, 4, and 10 mol. %) in the crystals are reported according to the dopant content in the initial mixture. The components were loaded into a 10 mm-diameter quartz ampoule, which was evacuated for 8 h at 300 °C to a residual pressure of 10^{-4} Torr. The sealed ampoule was placed in a high-temperature two-zone furnace. The melt was held for 12 h at a temperature of 20 °C above the melting point of $CsPbBr_3$ (567 °C). Subsequently, the ampoule was lowered through a region with a controlled temperature gradient at a rate of 2 mm/h. After completion of growth, the ampoule was annealed at 300 °C for 10 h and then cooled to room temperature over 30 h. Undoped $CsPbBr_3$ and $CdBr_2$-doped $CsPbBr_3$ crystals (0.5, 1, 4, and 10 mol. %) were grown. Photographs of the samples are presented in Appendix A (Fig. 8).

The elemental composition was analyzed using an ElvaX Pro x-ray fluorescence spectrometer. An x-ray spectrum was obtained with a Rh x-ray tube operating at an anode voltage of up to 60 kV and a current of up to 1000 μA, coupled with an SDD detector (Silicon Drift Detector) with an active area of 40 mm^2.

The sample morphology was examined by scanning electron microscopy (SEM) using a Tescan Vega3 LMU microscope. Surface imaging was performed with an electron beam generated by a W-thermocathode and accelerated to ∼20–30 kV. To verify the elemental composition of the crystals and to determine the component ratios, selected samples were analyzed by local x-ray microanalysis using an Oxford Instruments Aztec ONE energy-dispersive x-ray (EDX) system equipped with an X-MaxN20 detector. Elemental distribution across the sample surface was mapped using the same microanalyzer. SEM images of their surfaces (Figs. 9–11) and maps of the dopant distribution over the surface (Figs. 12–14) are provided in Appendix A.

The luminescence properties under synchrotron excitation were investigated at the experimental station of the P-66 Superlumi beamline (DESY, Hamburg).[30] Luminescence spectra were recorded using a Kymera 328i spectrograph with a 2 Å spectral slit and a CCD detector. The excitation radiation was provided by a McPherson normal-incidence monochromator with a 4 Å slit, covering the spectral range from 3.7 to 40 eV (UV–VUV region).

The luminescence decay kinetics were measured using the time-correlated single photon counting technique with a Hamamatsu R3809U-50 MCP-PMT detector. The effective time resolution, including the synchrotron pulse width and detector response, was 50 ps.

III. RESULT AND DISCUSSION

A. Phase composition and structure

The analysis of the diffraction pattern (Fig. 1) of the $CsPbBr_3$ crystal doped with 4 mol. % $CdBr_2$ revealed that the sample is single-phase and crystallizes in the orthorhombic system (space group *Pnma*). A reduction in the unit cell volume was observed for the doped crystal $CsPbBr_3$–4 mol. % $CdBr_2$ (a = 8.1683 Å, b = 8.2640 Å, c = 11.7002 Å, V = 789.81 $Å^3$) compared to the undoped one (a = 8.208 Å, b = 8.285 Å, c = 11.768 Å, V = 800.27 $Å^3$), amounting to 3.5%. Considering that the ionic radius of Cd^{2+} (∼95 pm) is smaller

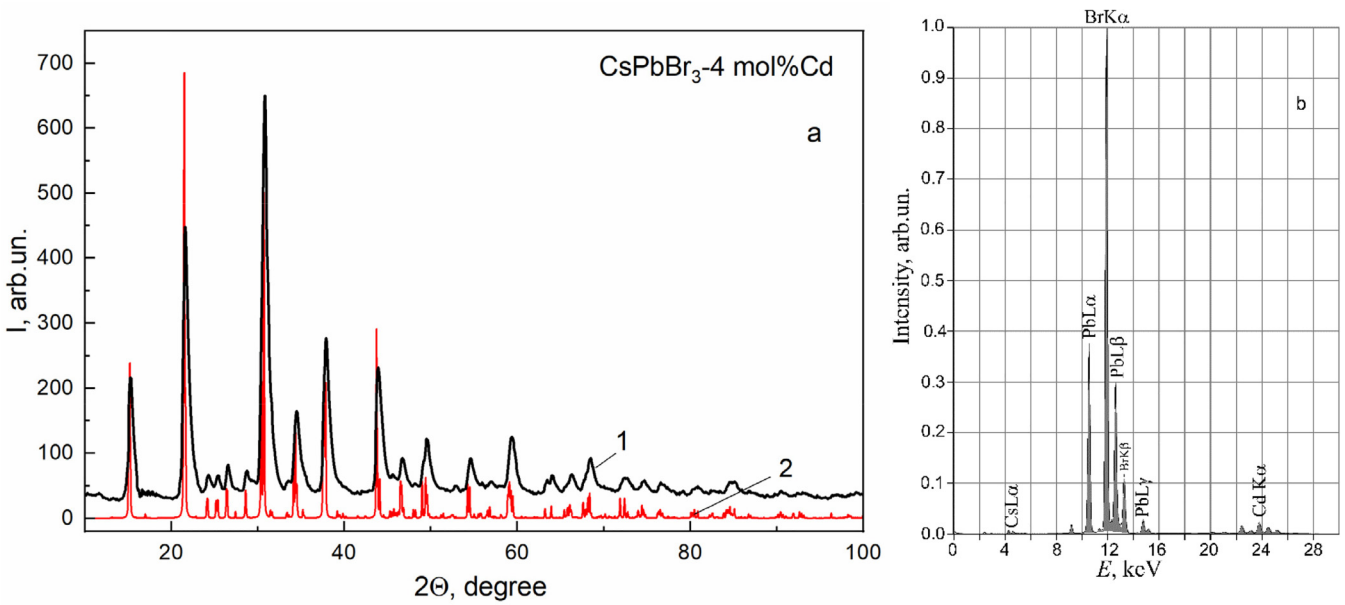

FIG. 1. (a) X-ray diffraction pattern of the $CsPbBr_3$ crystal doped with 4 mol. % $CdBr_2$ (curve 1). Curve 2 corresponds to the reference $CsPbBr_3$ pattern. (b) X-ray fluorescence spectrum of a $CsPbBr_3$ crystal grown with 4 mol. % $CdBr_2$.

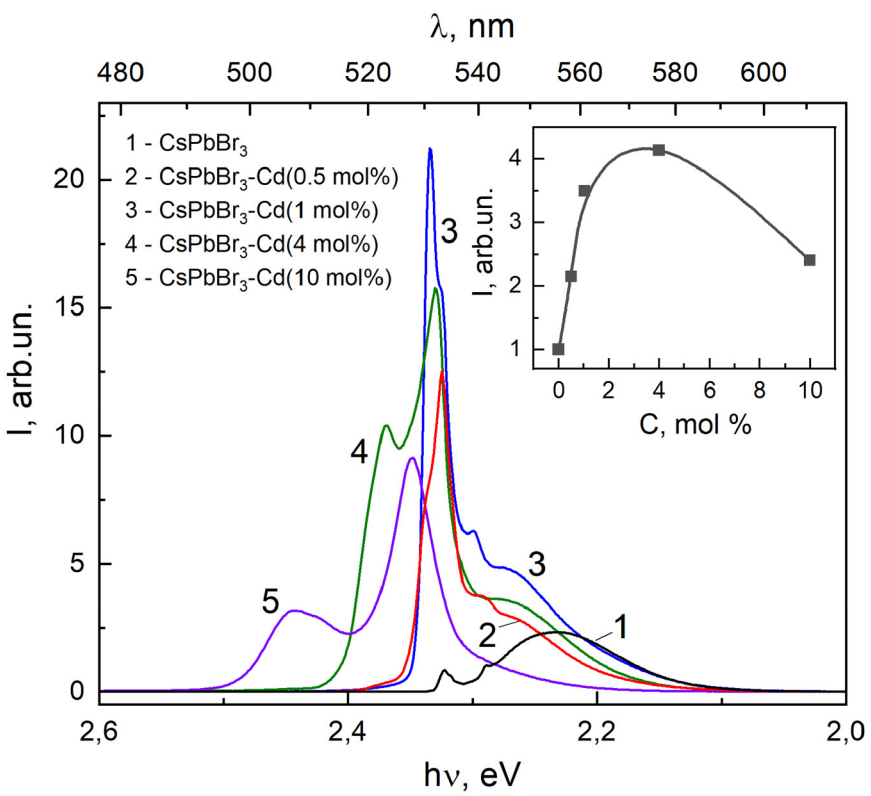

FIG. 2. Luminescence spectra of the $CsPbBr_3$ crystals with varying $CdBr_2$ concentrations measured at 8.2 K (λ_{ex} = 56 nm, 22.1 eV). Inset: Dependence of the luminescence intensity of the $CsPbBr_3$ crystals on the $CdBr_2$ concentration. The inset shows the tentative curve of the integrated intensity dependence of $CsPbBr_3$ near-edge luminescence on $CdBr_2$ concentration at a temperature of 8.2 K. Squares represent experimental results.

than that of Pb^{2+} (~119 pm) for a coordination number of 6, it can be inferred that cadmium ions substitute lead atoms in the $CsPbBr_3$ lattice. This substitution results in a contraction of the unit cell volume.

X-ray fluorescence (XRF) analysis performed with an ElvaX Pro spectrometer [Fig. 1(b)] confirmed that the Cs, Pb, and Br ratios in the grown crystals correspond to the stoichiometry of $CsPbBr_3$. The Cd content was found to be close to the nominal amount introduced into the raw material prior to crystal growth. Figure 1 presents the XRF spectrum of the $CsPbBr_3$ sample prepared with 4 mol. % $CdBr_2$ in the charge, corresponding to 3.7 mol. % Cd, as determined by XRF analysis.

B. Spectral and kinetic luminescence properties

1. Luminescence spectra

The luminescence spectrum of the pristine $CsPbBr_3$ single crystal [Fig. 2, curves 1 and Fig. 3(a), curve 1] under synchrotron excitation with photons of 22.1 eV ($\lambda_{ex} = 56$ nm) at 8.2 K exhibits two peaks in the short-wavelength region at 533.6 nm (2.323 eV, hereafter referred to as peak A) and 541.5 nm (2.289 eV, hereafter peak B), as well as a broad band centered at 556.3 nm (2.228 eV, hereafter peak C) with a full width at half maximum (FWHM) of 93 meV.

The luminescence spectra of the $CsPbBr_3$ single crystals exhibit features similar to those previously reported in Refs. 31–34. The narrow band A at 533.6 nm [Figs. 1 and 2(a)] is most often interpreted as the emission of free excitons.[32,34,35,36,19] In contrast, the nature of band B at 541.5 nm remains under discussion. This band has been attributed either to the luminescence of bound excitons localized at specific types of defects[37] or to emission associated with indirect transitions from Rashba minima[34,38] to the valence band. The interpretation of non-elementary long-wavelength band C at 556.3 nm (2.228 eV) is also ambiguous. It has been ascribed to the recombination of trapped excitons, donor–acceptor pairs, or self-trapped excitons.[32,34,35,39]

For $CdBr_2$ concentrations of 0.5 mol. % (Fig. 3, curve 2) and 1 mol. % (Fig. 3, curve 3), the position of the free exciton band remains essentially unchanged (Fig. 3, curve 1). This indicates that, within the impurity concentration range up to 1 mol. % $CdBr_2$, no significant modifications occur in the energy structure of the $CsPbBr_3$ crystal. A slight blue shift of band A (by 0.02–2.334 eV for 1 mol. % $CdBr_2$) can be attributed to changes in the crystal lattice parameters caused by the incorporation of Cd^{2+} ions, whose ionic radius (95 pm) is smaller than that of Pb^{2+} (~119 pm). At the same time, an increase is observed in both the integrated luminescence intensity (Fig. 2, inset) and the exciton emission intensity (Fig. 2), accompanied by a simultaneous decrease in the intensity of the C band.

For $CdBr_2$ impurity concentrations above 1 mol. %, bands A and B in $CsPbBr_3$ continue to broaden and shift toward the short-wavelength region, while the position of the broad luminescence band shifts from 556.3 nm (2.228 eV) to 545.1 nm (2.274 eV), accompanied by a decrease in its intensity. The integrated luminescence intensity of the $CsPbBr_3$ crystals increases fourfold at the $CdBr_2$ concentration of 4 mol. %, reaching a maximum (Fig. 2, inset). Based on the reported light yield of 3100 photons/MeV for

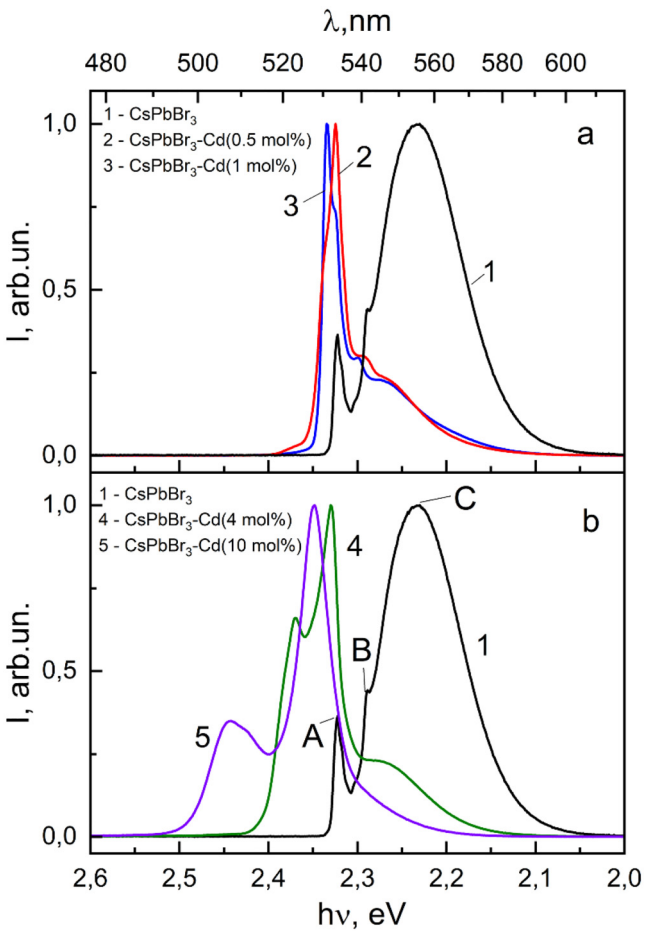

FIG. 3. Normalized luminescence spectra of the $CsPbBr_3$ crystals with varying $CdBr_2$ concentrations measured at 8.2 K ($\lambda_{ex} = 56$ nm, 22.1 eV): (a) 1—0 mol. %, 2—0.5 mol. %, and 3—1 mol. %; (b) 1—0 mol. %, 2—4 mol. %, and 3—10 mol. %.

exciton emission at 538 nm with decay time constant ($\tau_1 = 0.44$ ns)[19] for undoped $CsPbBr_3$ and taking into account the approximately fourfold enhancement of exciton luminescence intensity observed in this study, the light yield of excitonic luminescence at 534 nm ($\tau_1 = 0.45$ ns) for $CsPbBr_3$ doped with 4 mol. % $CdBr_2$ is expected to reach approximately 12 400 photons/MeV at 10 K. This is a highly encouraging result, particularly in view of the fast decay times.

With increasing $CdBr_2$ concentration up to 10 mol. % in the $CsPbBr_3$ crystal, the trend of the exciton-like luminescence musicum shifting toward the short-wavelength region continues, reaching 527.9 nm (2.348 eV). The intensity of band C continues to decrease and is significantly quenched at the $CdBr_2$ concentration of 10 mol. % [Figs. 2 and 3(b), curve 5].

The observed blue shift of the luminescence bands in the $CsPbBr_3$ single crystals upon doping with $CdBr_2$ is a characteristic feature of near-edge luminescence in lead halide perovskite nanoparticles activated by metal cations.[17,40,41]

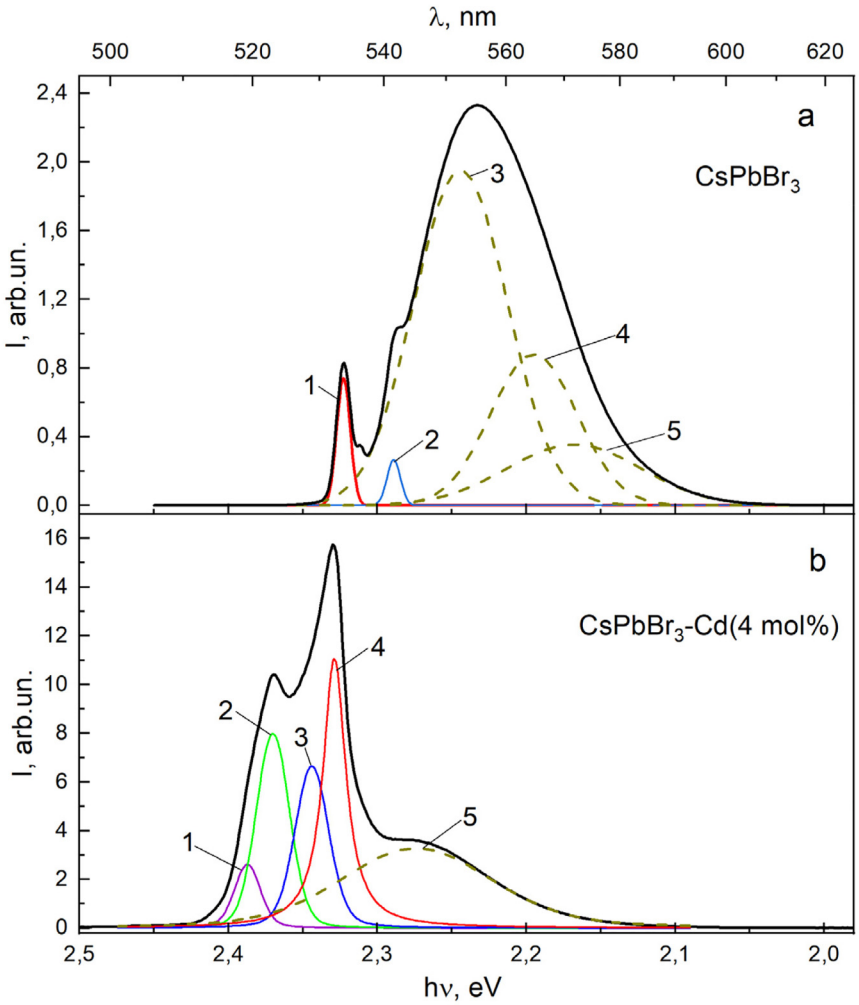

FIG. 4. Decomposition of the luminescence band of $CsPbBr_3$ (a) and $CsPbBr_3$–4 mol. % $CdBr_2$ (b) into components at a temperature of 8.2 K.

A more detailed analysis of the modification of the luminescence spectra of the $CsPbBr_3$ crystals induced by $CdBr_2$ doping (Fig. 4) was carried out using spectral curve decomposition into individual components.

In the undoped $CsPbBr_3$ crystal [Fig. 4(a)], emission bands can be distinguished at 2.322 eV (band 1), 2.289 eV (band 2), 2.245 eV (band 3), 2.195 eV (band 4), and 2.168 eV (band 5) (Table I). The first two bands correspond to the emission of the free exciton (band A) and the Rashba exciton (band B), respectively. Their FWHM does not exceed 12.5 meV, in agreement with the data reported in Ref. 34. The non-elementary band C can be approximated by bands 3, 4, and 5, with FWHM values ranging from 70 to 150 meV.

Decomposition into constituent components was also performed for the $CsPbBr_3$ crystal with 4 mol. % $CdBr_2$ impurity, which exhibits the maximum intensity of near-edge luminescence [Fig. 4(b)]. In the emission spectrum, four exciton-like narrow bands can be distinguished: 1–2.329 eV, 2–2.388 eV, 3–2.371 eV, and 4–2.344 eV [Fig. 4(b), Table I], with FWHM below 28 meV, along with a broad band 5 at 2.274 eV with a FWHM of 223 meV.

TABLE I. The decomposition parameters of the $CsPbBr_3$ and $CsPbBr_3$–4 mol. % $CdBr_2$ near-edge luminescence spectrum at a temperature of 8.2 K. E_{max} represents the position of the maximum of the band and ΔE represents the half-width of the band.

Peak number	E_{max} (eV)	ΔE (meV)
$CsPbBr_3$		
1	2.322	12.3
2	2.289	10.2
3	2.245	74.0
4	2.195	63.1
5	2.168	150.0
$CsPbBr_3$–4 mol. % $CdBr_2$		
1	2.388	21.6
2	2.371	13.8
3	2.344	27.8
4	2.329	18.5
5	2.274	223.1

In the impurity concentration range up to 1 mol. %, the $CsPbBr_3$ crystal can be considered weakly activated, as the introduction of the dopant does not significantly affect the position of the fundamental absorption edge of the crystal. For $CdBr_2$ concentrations of 4 and 10 mol. % in $CsPbBr_3$, the absorption edge shift becomes noticeable, reaching 46 and 119 meV, respectively, suggesting the possible formation of a solid solution $CsPb_{1-x}Cd_xBr_3$. At the same time, no evidence for the formation of $CsCdBr_3$ crystalline phase was found based on the luminescence parameters.[42] The formation of solid solutions over a wide range of activator concentrations is a characteristic feature of halide perovskites.

The introduction of $CdBr_2$ not only leads to the formation of defects responsible for the appearance of additional near-edge luminescence bands but also reduces the number of defects that quench exciton luminescence. The additional incorporation of Cd and Br into the lattice is expected to decrease the number of lead cation vacancies and bromine anion vacancies, which are the main quenchers of exciton emission. Considering that the Pb–Br bond length in hexagonal $CsPbBr_3$ (2.99 Å[43]) is larger than the Cd–Br bond length in hexagonal $CsCdBr_3$ (2.79 Å[44]) and that the electronegativity difference of Pb–Br (0.63) is smaller than that of Cd–Br (1.27), it is reasonable to assume a higher degree of ionic character for the Cd–Br bond and, correspondingly, a higher bond energy of Cd–Br compared to Pb–Br. The results of quantum mechanical calculations in the density functional theory (DFT) approximation show that the formation energy of a bromine vacancy is 2.91 eV for pure $CsPbBr_3$ and increases to 6.41–7.12 eV in Cd-doped $CsPbBr_3$, depending on the relative position of the bromine vacancy with respect to the Cd impurity (see Appendix B). The higher formation energy of a bromine vacancy in the Cd-doped $CsPbBr_3$ crystal compared to the pure one contributes to the reduction of bromine vacancies. This promotes the stabilization of the $CsPbBr_3$ lattice against the formation of bromine vacancies. The ordering of the $CsPbBr_3$ matrix is also evidenced by the increase in the tolerance factor from 0.815 for $CsPbBr_3$ to 0.882 for $CsCdBr_3$ upon substitution of Pb with Cd. Therefore, the emergence of additional exciton-like bands, apart from the free exciton band, can be attributed to exciton scattering by defects introduced through doping.

In addition to the exciton-like edge luminescence in the visible region described above, the $CsPbBr_3$ crystals exhibit broadband luminescence in the infrared spectral region under excitation with synchrotron radiation at photon energies of 7.51 eV, with a maximum at 920 nm (Fig. 5).

Previously, this infrared luminescence (800–1050 nm) was reported by Dorenbos[19] and is excited by x rays but not by photons with energies below 10 eV. In the present study, under excitation

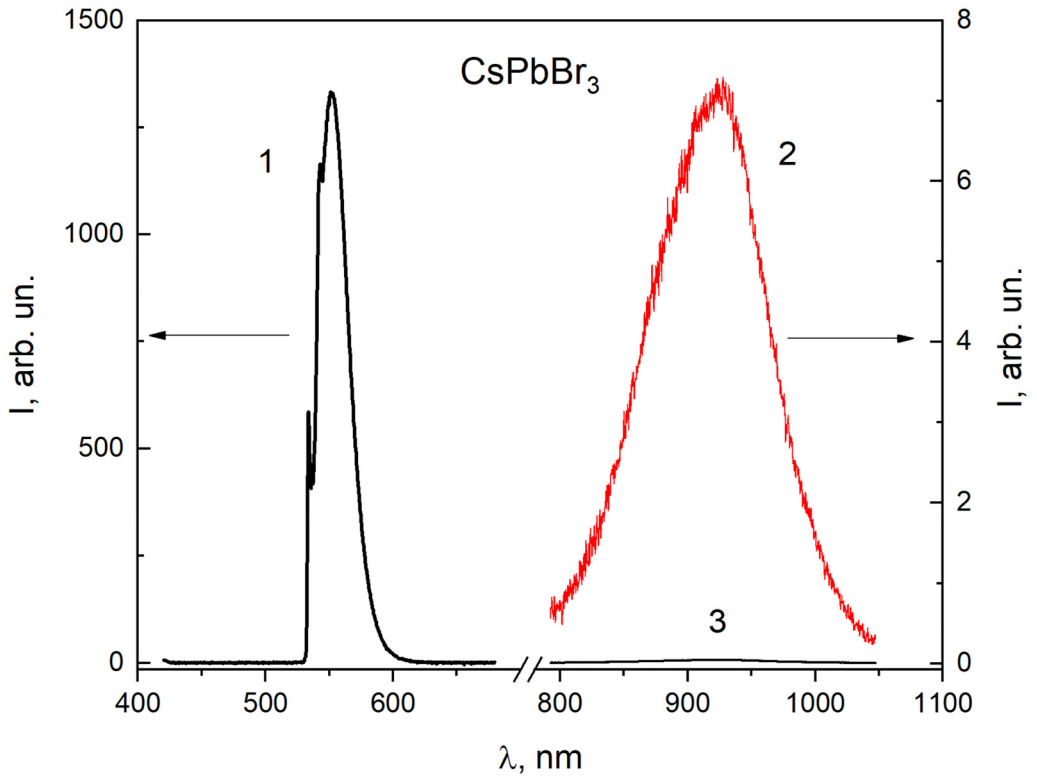

FIG. 5. Luminescence spectra of the undoped $CsPbBr_3$ crystal (curves 1 and 3—on the same scale); curve 2—luminescence spectrum in the infrared region on an enlarged scale (right-hand axis). T = 8.2 K. Excitation photon energy $h\nu_{ex}$ = 7.51 eV (λ_{ex} = 160 nm).

with 8.8 eV synchrotron photons, we observed the same long-wavelength luminescence in the $CsPbBr_3$ crystals, with a maximum at 920 nm (Fig. 5). However, its intensity, as evident from the comparison of curves 1 and 3, is negligible. The possibility that this luminescence may originate from excitation by high-energy scattered light cannot be excluded. It is more likely, however, that the luminescence originates from the emission of radiation-induced defects, as suggested in Ref. 19 and evidenced by the luminescence of F-centers in the $CsPbCl_3$ crystals. With increasing irradiation dose, the broadband F-centers' luminescence at 555 nm in $CsPbCl_3$ significantly increased in intensity.[19] Based on this luminescence mechanism, the weak infrared emission of $CsPbBr_3$ under synchrotron excitation can be explained by the lower probability of generating radiation defects. This is evident because the probability of defect formation under x-ray irradiation is higher than that under synchrotron excitation. Synchrotron radiation is predominantly absorbed near the surface, whereas x rays are absorbed throughout the crystal volume. Consequently, the formation of radiation-induced defects is considerably more probable under x-ray excitation than under synchrotron irradiation.

2. Time parameters of near-edge luminescence

For the undoped $CsPbBr_3$ single crystal, the decay time kinetics of the luminescence intensity for the free exciton band (533.6 nm, 2.323 eV) consists of two components, $\tau_1 = 0.36$ ns and $\tau_2 = 2.69$ ns (Fig. 6, Table II). The time parameters for doped crystals were measured for the bands with the maximum intensity (Table II). The contribution of the fast decay component τ_1 to the luminescence pulse is predominant for all crystals. With increasing dopant concentration, the average decay constant, calculated according to the formula $\tau_{aver} = \frac{\tau_1 A_1 + \tau_2 A_2}{A_1 + A_2}$, decreases from 0.47 ns (undoped crystal) to 0.23 ns (0.5 mol. % $CdBr_2$). For higher cadmium concentrations, the average decay constant of $CsPbBr_3$ varies within 0.41–0.73 ns. In contrast, the non-elementary C-band is likely characterized by a decay time in the microsecond range, as previously reported in Ref. 33.

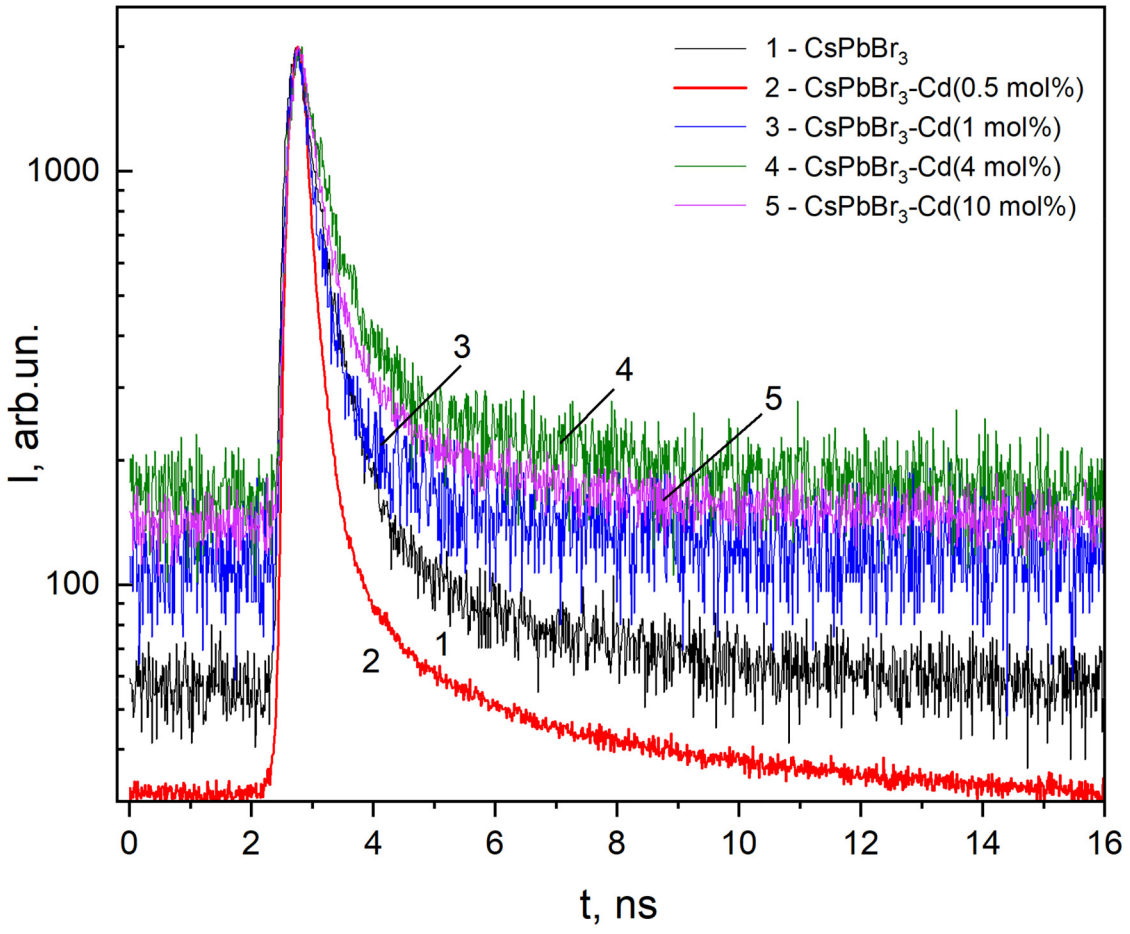

FIG. 6. Decay time kinetics curves of the $CsPbBr_3$ luminescence intensity as a function of $CdBr_2$ concentration. T = 8.2 K, $h\nu_{ex}$ = 7.51 eB (λ_{ex} = 160 нм).

TABLE II. Fast and slow components of the luminescence decay kinetics of $CsPbBr_3$ depending on the concentration of $CdBr_2$ at a temperature of 8.2 K and λ_{ex} = 160 нм.

Compound	λ_{em} (nm)	τ_1 (ns)	A_1	τ_2 (ns)	A_2	τ_{aver} (ns)
$CsPbBr_3$	534	0.36	1924	2.69	98	0.47
$CsPbBr_3$–0.5 mol. % $CdBr_2$	532	0.17	2654	1.54	124	0.23
$CsPbBr_3$–1 mol. % $CdBr_2$	532	0.26	1688	2.25	141	0.41
$CsPbBr_3$–4 mol. %$CdBr_2$	532	0.45	1455	3.35	155	0.73
$CsPbBr_3$–10 mol. %$CdBr_2$	529	0.32	1669	2.13	207	0.52

3. Excitation spectra of near-edge luminescence

Normalized excitation spectra of luminescence for the undoped (curve 1) and the 4 mol. % $CdBr_2$-doped (curve 2) $CsPbBr_3$ crystals in the energy range of 4–10 eV are shown in Fig. 7. The normalized luminescence excitation spectrum of the 4 mol. % $CdBr_2$-doped $CsPbBr_3$ crystal (curve 2) reproduces the features (peaks and dips) characteristic of the undoped $CsPbBr_3$ crystal (curve 1). The retention of the excitation band positions for the 4 mol. % $CdBr_2$-doped crystal in the 6.2–10 eV energy range indicates only minor changes in the energy band structure of $CsPb_{1-x}Cd_xBr_3$. However, in the spectral region of 4.5–6.2 eV (275–200 nm), changes in the luminescence excitation efficiency are observed, as clearly reflected by curve 3, which represents the ratio of the normalized excitation spectra of the doped $CsPbBr_3$–4 mol. % $CdBr_2$ to the undoped crystal. In this spectral region, the excitation of luminescence is most efficient.

It should be noted that if the luminescence enhancement were uniform across all wavelengths, this ratio would be equal to 1 and would appear as a straight line. In our case, for the energy range of 6.2–10 eV (curve 3), the ratio is close to unity, whereas in the 4.5–6.2 eV energy range, the excitation efficiency of the doped crystal increases, reaching a maximum that is approximately twice as high. This difference may be associated with changes in the density of states of the conduction band upon cadmium incorporation. It is evident that more accurate results regarding the luminescence enhancement in Cd-doped $CsPbBr_3$ can be obtained under x-ray excitation, which is absorbed throughout the crystal volume, in contrast to synchrotron excitation, which is predominantly absorbed at the sample surface.

IV. SUMMARY

In the Cd-doped $CsPbBr_3$ single crystals, under excitation by synchrotron quanta with an energy of hν = 7.747 eV (160 nm), in addition to exciton luminescence, the appearance of additional emission bands is observed, caused by the exciton scattering at lattice defects. The luminescence decay time constants remain at the level of the undoped crystal, the near-edge luminescence bands shift toward higher energies, and the edge exciton luminescence intensity increases by a factor of 4.

The incorporation of cadmium ions into the $CsPbBr_3$ single crystals over stoichiometric levels reduces the number of bromine

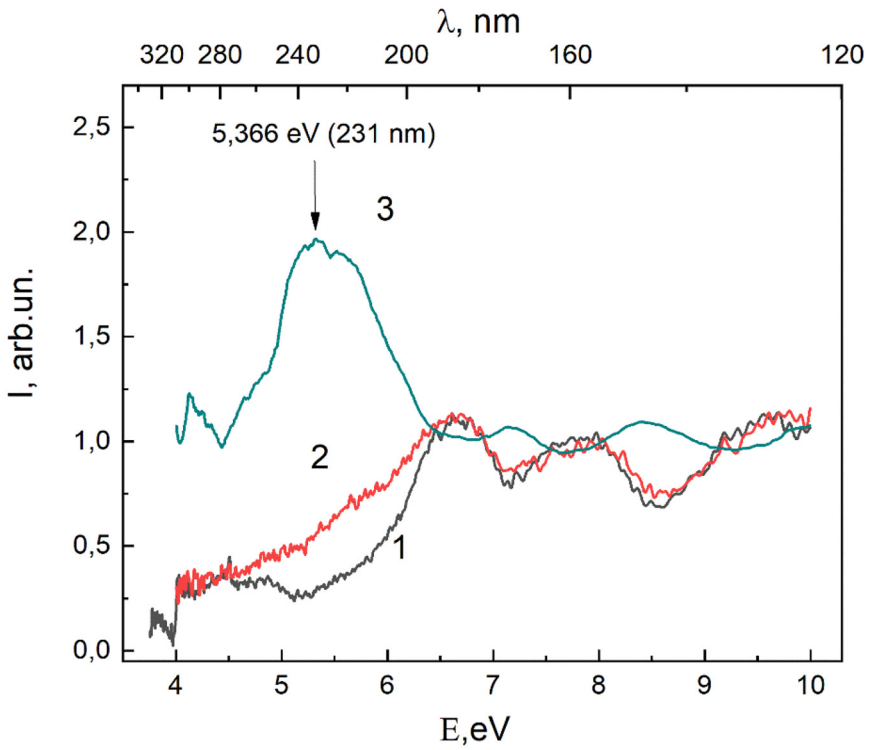

FIG. 7. Normalized luminescence excitation spectra of the $CsPbBr_3$ crystals with different $CdBr_2$ concentrations (1—undoped; 2—4 mol. % $CdBr_2$; 3—ratio of curve 2 to curve 1). T = 8.2 K.

vacancies, increases the formation energy of anion vacancies in the Cd–Br pair, which acts as a diffusion barrier for chloride ions, and improves the tolerance factor of the perovskite lattice. This leads to the elimination of non-radiative relaxation pathways during electron thermalization and reduces exciton energy transfer to non-radiative centers.

In addition to near-edge luminescence, infrared luminescence is detected, which is most likely associated with the emission from radiation-induced defects.

The significant enhancement of exciton luminescence in the cadmium-activated $CsPbBr_3$ crystal, with decay time constants of ~0.5 ns remaining at the level of the undoped crystal, opens prospects for the development of fast cryogenic scintillators with sufficiently high light yield at the level of 12 400 photons/MeV at the temperature of 10 K based on the $CsPbBr_3$ matrix.

ACKNOWLEDGMENTS

We acknowledge DESY (Hamburg, Germany), a member of the Helmholtz Association HGF, for the provision of experimental facilities carried out at PETRA III using beamline P66 operated by DESY Photon Science. Beamtime was allocated for Proposal No. I-20230140 EC. The research leading to this result has been co-funded by the project NEPHEWS under Grant Agreement No. 101131414 from the EU Framework Programme for Research and Innovation Horizon Europe (T.D., R.G., and A.P.). The work was partially supported by the Ministry of Education and Science of Ukraine (Grant No. 0125U002198) and has received funding through the EURIZON project, which is funded by the European Union under Grant Agreement No. 871072.

AUTHOR DECLARATIONS

Conflict of Interest

The authors have no conflicts to disclose.

Author Contributions

V. Shvets: Data curation (equal); Formal analysis (equal). **A. Pushak:** Investigation (equal); Writing – original draft (equal). **O. Antonyak:** Data curation (equal); Formal analysis (equal); Investigation (equal). **R. Gamernyk:** Investigation (equal). **A. Kotlov:** Investigation (equal); Methodology (equal). **Y. Smortsova:** Investigation (equal); Methodology (equal). **V. Salapak:** Investigation (equal); Methodology (equal); Resources (equal). **A. Zelinskiy:** Data curation (equal); Investigation (equal); Resources (equal). **V. Stakhura:** Data curation (equal); Investigation (equal); Visualization (equal). **O. Bovgyra:** Software (equal). **T. Demkiv:** Data curation (equal); Investigation (equal); Software (equal); Visualization (equal); Writing – original draft (equal); Writing – review & editing (equal). **A. Voloshinovskii:** Conceptualization (equal); Supervision (equal); Writing – original draft (equal); Writing – review & editing (equal).

DATA AVAILABILITY

The data that support the findings of this study are available from the corresponding author upon reasonable request.

APPENDIX A: CHARACTERIZATION OF THE GROWN Cd^{2+}-DOPED $CsPbBr_3$ SINGLE CRYSTALS

1. Photographs of the grown crystals

See Fig. 8.

2. SEM images of the sample surface

See Fig. 9.

3. SEM–EDS elemental maps acquired from the sample surface

See Figs. 10–14.

APPENDIX B: INFLUENCE OF CADMIUM DOPING ON THE FORMATION ENERGY OF BROMINE VACANCIES

We investigated the effect of Cd-doping on the structural stability of the perovskite by calculating the formation energy of the Br vacancy (V_{Br}). Total energy calculations were performed using the density functional theory (DFT) implemented in the CASTEP package based on pseudopotential plane-wave methods.[45] We apply the Perdew–Burke–Ernzerhof (PBE) parametrization for generalized gradient approximation (GGA) to describe the exchange-correlation functional. After convergence tests, the plane-wave basis set cutoff energy was set as 450 eV; the convergence tolerance for energy was set as 5×10^{-6} eV/atom, and the tolerance for maximum force was 0.01 eV/Å. A $2 \times 2 \times 2$ supercell was used to simulate the $CsPbBr_3$ substitutional doping system. First, we provide geometry optimization of the undoped $CsPbBr_3$ crystal using the

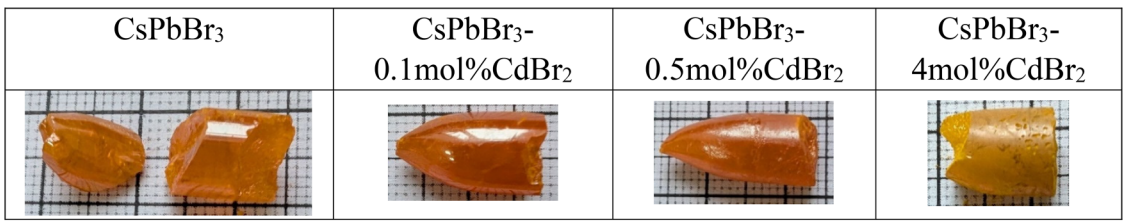

FIG. 8 Photographs of the grown $CsPbBr_3$ crystals without and with cadmium impurities.

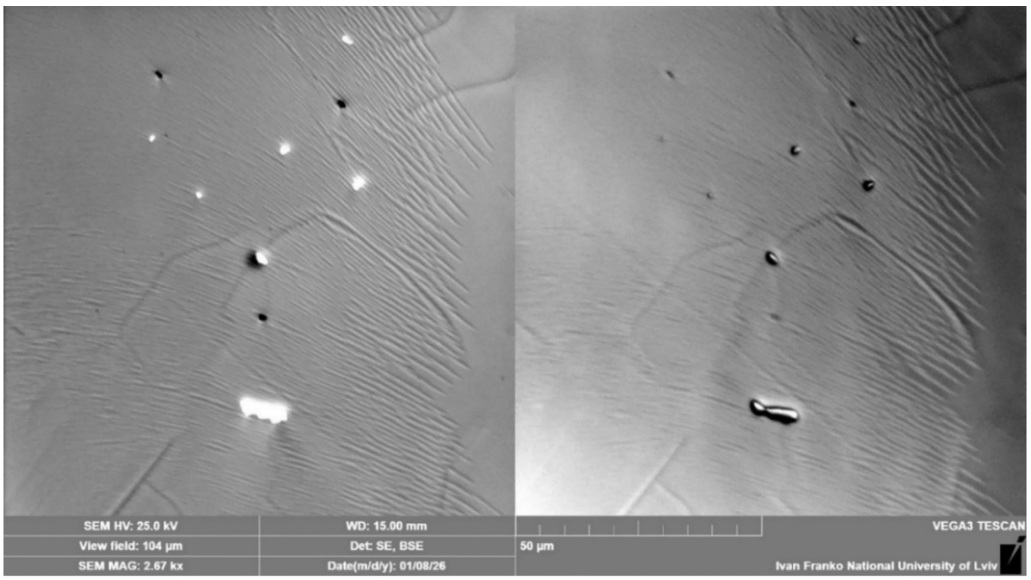

FIG. 9. $CsPbBr_3$ crystal surface imaged in (a) secondary electron (SE) and (b) backscattered electron (BSE) modes.

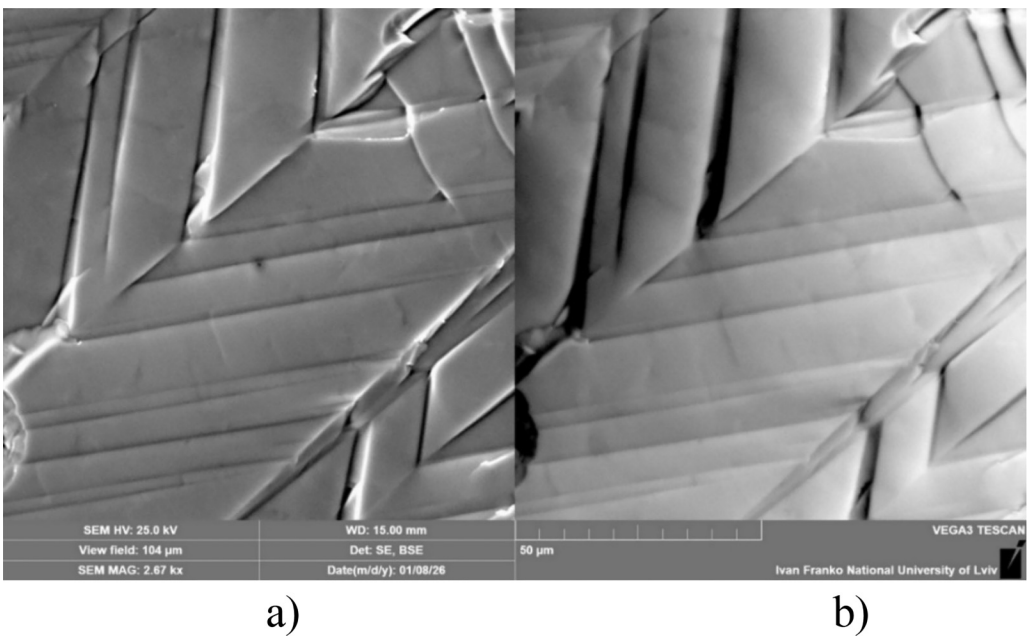

FIG. 10. $CsPbBr_3$–1 mol. % $CdBr_2$ crystal surface imaged in (a) secondary electron (SE) and (b) backscattered electron (BSE) modes.

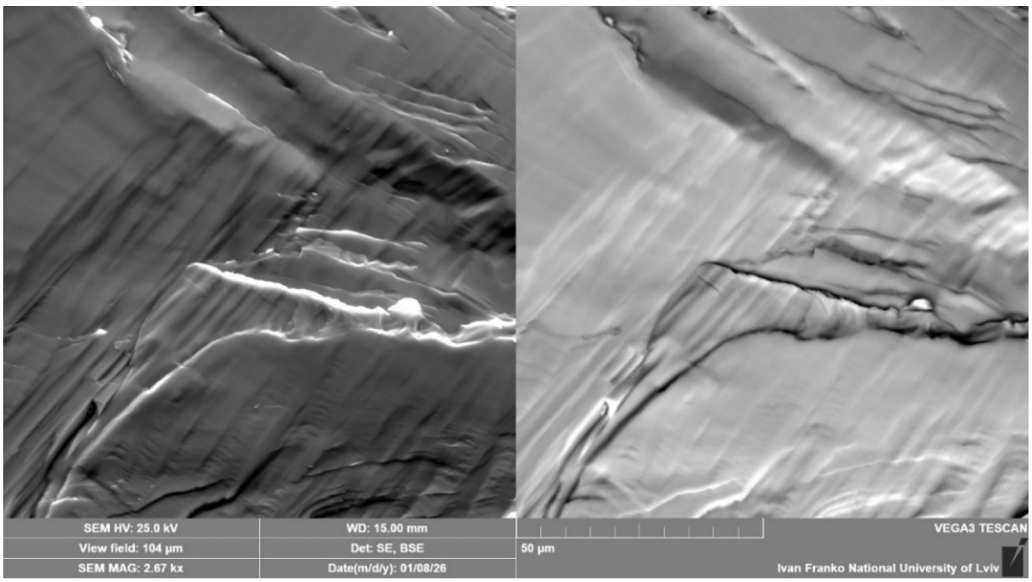

FIG. 11. $CsPbBr_3$–4 mol. % $CdBr_2$ crystal surface imaged in (a) secondary electron (SE) and (b) backscattered electron (BSE) modes.

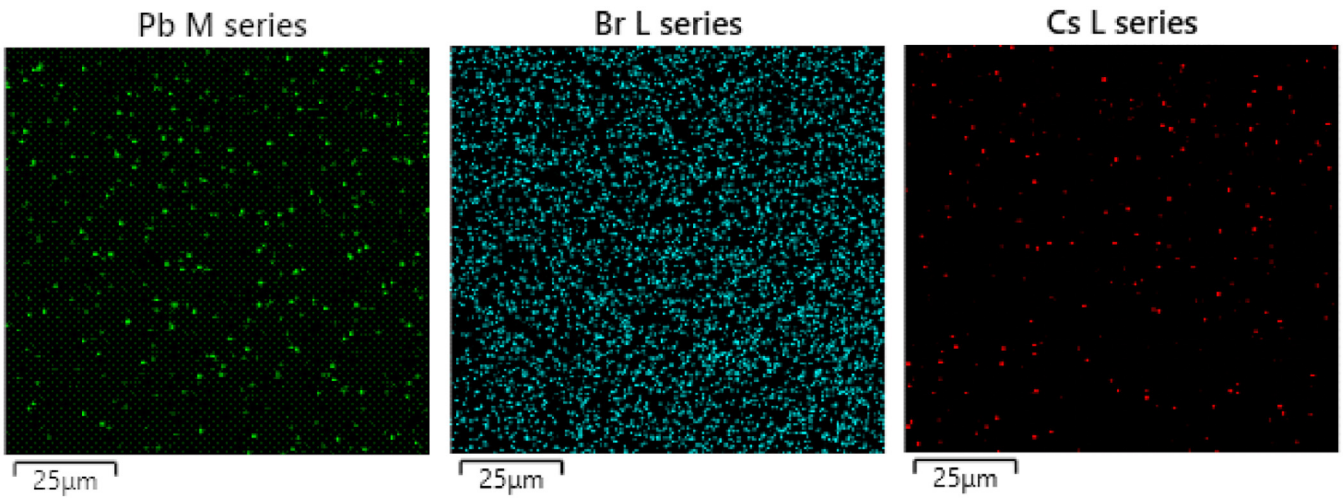

FIG. 12. SEM–EDS elemental maps of Pb, Br, and Cs acquired from the sample surface of $CsPbBr_3$ crystal.

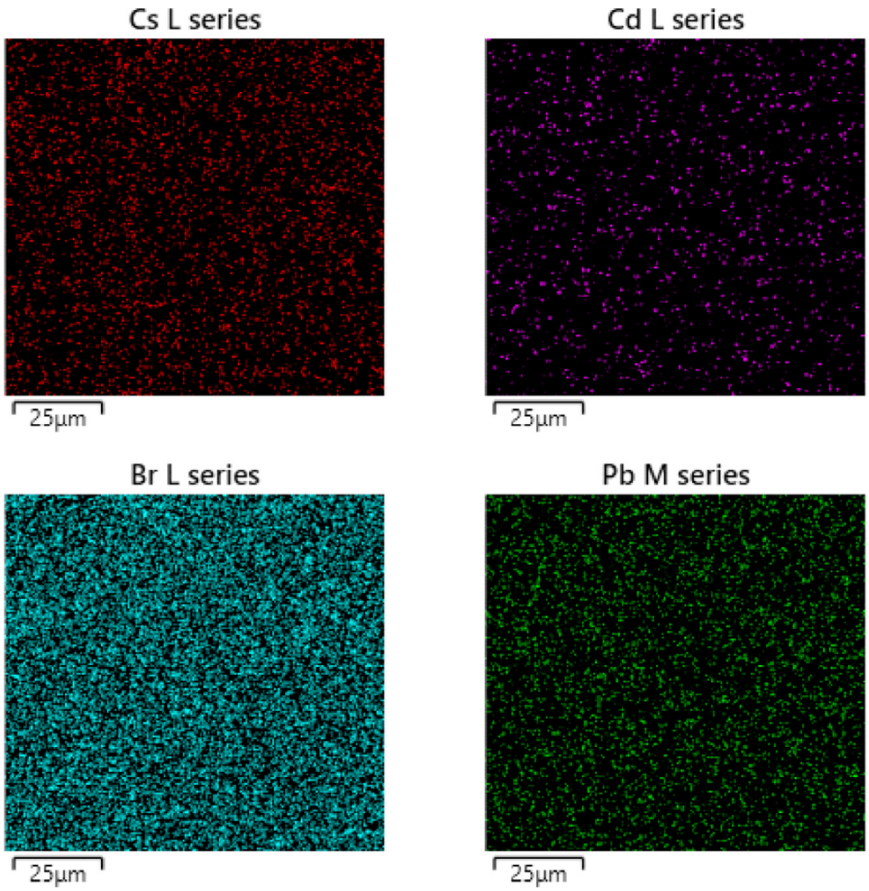

FIG. 13. SEM–EDS elemental maps of Cs, Pb, Br, and Cd acquired from the sample surface of the $CsPbBr_3$–1 mol. % $CdBr_3$ crystal.

effective Broyden–Fletcher–Goldfarb–Shanno algorithm. Next, we substituted one Pb atom in the supercell with a Cd atom, and the optimization procedure was repeated using the same algorithm. The interactions between the atomic core and valence electrons were described using ultrasoft pseudopotentials.

To calculate the formation energy of bromine vacancies in $CsPbBr_3$, a supercell model ($2 \times 2 \times 2$) of the cubic perovskite structure was constructed, and bromine vacancies were introduced by removing a single Br atom, followed by full geometry optimization. For Cd-doped systems, a Pb atom was substituted by Cd^{2+}, and the Br vacancy was created at various positions relative to the dopant to analyze coordination effects.

The vacancy formation energy (E_{vac}) was calculated using the following expression:

$$E_{vac} = E_{s-vac} + E_{Br} - E_s, \tag{B1}$$

where E_s is the total energy of the supercell $CsPbBr_3$ without a vacancy, E_{s-vac} is that of the supercell with a vacancy, and E_{Br} is 1/2 of the total energy of the Br_2 molecule in the gas phase.

The study of perovskite stability in relation to point defects is critical, given their substantial influence on electronic and optical properties. Computational results show that the formation energy of a bromine vacancy (E_{vac}) is 2.91 eV for pristine $CsPbBr_3$ and 6.41–7.12 eV for Cd-doped $CsPbBr_3$ (depending on the position of the chlorine vacancy relative to the Cd dopant ion, where higher formation energy is characteristic of bromine vacancies located closer to cadmium). The positive values confirm that vacancy formation is endothermic in both materials. Our results on the formation energies of chlorine vacancies are consistent with the data reported in Ref. 46; in particular, the formation energy of V_{Br} in the pristine crystal is 3.32 eV.

The observation that the vacancy formation energy is higher in the Cd-doped perovskite than in the undoped structure is highly significant. This result implies that introducing Cd as a dopant makes the formation of Br vacancy less thermodynamically favorable. This finding can be directly interpreted as the Cd dopant stabilizing the perovskite structure. Essentially, the presence of Cd atoms enhances the lattice's overall structural integrity, thereby reducing the likelihood of point defects.

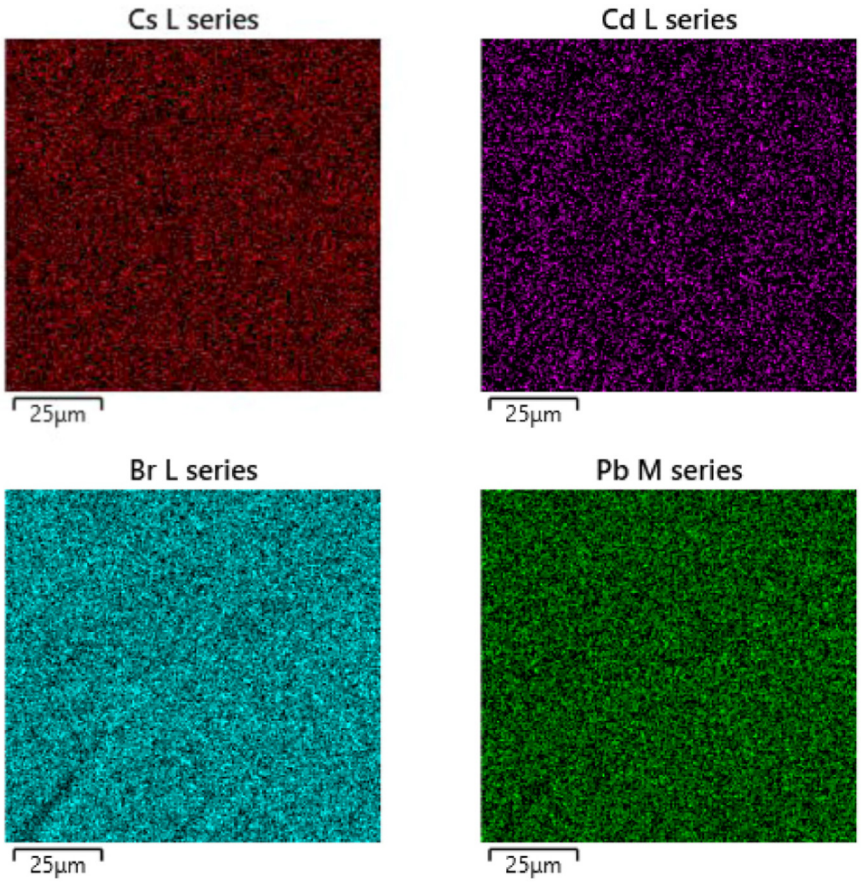

FIG. 14. SEM–EDS elemental maps of Cs, Pb, Br, and Cd acquired from the sample surface of the $CsPbBr_3$–4 mol. % $CdBr_3$ crystal.

REFERENCES

[1]L. Protesescu, S. Yakunin, M. I. Bodnarchuk, F. Krieg, R. Caputo, C. H. Hendon, R. X. Yang, A. Walsh, and M. V. Kovalenko, "Nanocrystals of cesium lead halide perovskites ($CsPbX_3$, X = Cl, Br, and I): Novel optoelectronic materials showing bright emission with wide color gamut," Nano Lett. **15**, 3692–3696 (2015).

[2]A. A. M. Brown, B. Damodaran, L. Jiang, J. N. Tey, S. H. Pu, N. Mathews, and S. G. Mhaisalkar, "Lead halide perovskite nanocrystals: Room temperature syntheses toward commercial viability," Adv. Energy Mater. **10**, 2001349 (2020).

[3]H. Yuce, M. Mandal, Y. Yalcinkaya, D. Andrienko, and M. M. Demir, "Improvement of photophysical properties of $CsPbBr_3$ and Mn^{2+}:$CsPb(Br,Cl)_3$ perovskite nanocrystals by Sr^{2+} doping for white light-emitting diodes," J. Phys. Chem. C **126**, 11277–11284 (2022).

[4]X. Y. Chin, D. Cortecchia, J. Yin *et al.*, "Lead iodide perovskite light-emitting field-effect transistor," Nat. Commun. **6**, 7383 (2015).

[5]Z.-K. Tan *et al.*, "Bright light-emitting diodes based on organometal halide perovskite," Nat. Nanotechnol. **9**, 687–692 (2014).

[6]T. Guner and M. M. Demir, "A review on halide perovskites as color conversion layers in white light emitting diode applications," Phys. Status Solidi A **215**, 1800120 (2018).

[7]R. X. Lin, J. Xu, M. Y. Wei, Y. R. Wang, Z. Y. Qin, Z. Liu, J. L. Wu, K. Xiao, B. Chen, S. M. Park *et al.*, "All-perovskite tandem solar cells with improved grain surface passivation," Nature **603**, 73–78 (2022).

[8]H. Min, D. Y. Lee, J. Kim, G. Kim, K. S. Lee, J. Kim, M. J. Paik, Y. K. Kim, K. S. Kim, M. G. Kim *et al.*, "Perovskite solar cells with atomically coherent interlayers on SnO_2 electrodes," Nature **598**, 444–450 (2021).

[9]Z. L. Chen, B. Turedi, A. Y. Alsalloum, C. Yang, X. P. Zheng, I. Gereige, A. Alsaggaf, O. F. Mohammed, and O. M. Bakr, "Single-crystal $MAPbI_3$ perovskite solar cells exceeding 21% power conversion efficiency," ACS Energy Lett. **4**, 1258–1259 (2019).

[10]A. Y. Alsalloum, B. Turedi, X. P. Zheng, S. Mitra, A. A. Zhumekenov, K. J. Lee, P. Maity, I. Gereige, A. Alsaggaf, I. S. Rogan *et al.*, "Low-temperature crystallization enables 21.9% efficient single-crystal $MAPbI_3$ inverted perovskite solar cells," ACS Energy Lett. **5**, 657–662 (2020).

[11]R. Chen, J. Li, W. Zhao, and Y. Lei, "Halide perovskite single crystals: Progress, challenges, and future perspectives," Mater. Today Electron. **15**, 100193 (2026).

[12]H. Wei, Y. Fang, P. Mulligan, W. Chuirazzi, H.-H. Fang, C. Wang, B. R. Ecker, Y. Gao, M. A. Loi, L. Cao *et al.*, "Sensitive X-ray detectors made of methylammonium lead tribromide perovskite single crystals," Nat. Photonics **10**, 333–339 (2016).

[13]X. Wang, Y. W. Li, Y. B. Xu, Y. Z. Pan, C. Y. Zhu, D. J. Zhu, Y. Wu, G. W. Li, Q. Zhang, Q. Li *et al.*, "Solution-processed halide perovskite single crystals with intrinsic compositional gradients for X-ray detection," Chem. Mater. **32**, 4973–4983 (2020).

[14]Z. Liu, J. A. Peters, C. C. Stoumpos, M. Sebastian, B. W. Wessels, J. Im, A. J. Freeman, and M. G. Kanatzidis, "Heavy metal ternary halides for room-temperature X-ray and gamma-ray detection," Proc. SPIE **8852**, 88520A (2013).

[15]C. C. Stoumpos, C. D. Malliakas, J. A. Peters, Z. Liu, M. Sebastian, J. Im, T. C. Chasapis, A. C. Wibowo, D. Y. Chung, A. J. Freeman,

B. W. Wessels, and M. G. Kanatzidis, Cryst. Growth Des. **13**, 2722 (2013).
[16]V. B. Mykhaylyk, H. Kraus, V. Kapustianyk, H. J. Kim, P. Mercere, M. Rudko, P. Da Silva, O. Antonyak, and M. Dendebera, "Bright and fast scintillations of an inorganic halide perovskite $CsPbBr_3$ crystal at cryogenic temperatures," Sci. Rep. **10**, 8601 (2020).
[17]O. Pidhornyi, Y. Chornodolskyy, A. Pushak, Y. Smortsova, A. Kotlov, O. Antonyak, T. Demkiv, R. Gamernyk, and A. Voloshinovskii, "Enhancement of near edge luminescence in cadmium ions doped $CsPbCl_3$ single crystals," J. Appl. Phys. **134**, 135105 (2023).
[18]G. H. Ahmed, J. Yin, O. M. Bakr, and O. F. Mohammed, "Near-unity photoluminescence quantum yield in inorganic perovskite nanocrystals by metal-ion doping," J. Chem. Phys. **152**, 020902 (2020).
[19]J. J. van Blaaderen, D. Biner, K. W. Krämer, and P. Dorenbos, "The temperature dependent optical and scintillation characterisation of Bridgman grown $CsPbX_3$ (X = Br, Cl) single crystals," Nucl. Instrum. Methods Phys. Res. **1064**, 169322 (2024).
[20]K. Watanabe, M. Koshimizu, T. Yanagida, Y. Fujimoto, and K. Asai, "Luminescence and scintillation properties of La- and La,Ag-doped $CsPbCl_3$ single crystals," Jpn. J. Appl. Phys. **55**, 02BC20 (2016).
[21]Z. Xu, L. Qian, S. Wu, Q. Wang, P. Hu, S. Pan, and J. Pan, "Growth, luminescence and photoelectrical properties of $Cs_{1-x}Li_xPbCl_3$ ($0 \le x < 1$) single crystals," J. Cryst. Growth **673**, 128392 (2026).
[22]S. Das, A. De, and A. Samanta, "Ambient condition Mg^{2+} doping producing highly luminescent green- and violet-emitting perovskite nanocrystals with reduced toxicity and enhanced stability," J. Phys. Chem. Lett. **11**, 1178–1188 (2020).
[23]J.-S. Yao, J. Ge, B.-N. Han, K.-H. Wang, H.-B. Yao, H.-L. Yu, J.-H. Li, B.-S. Zhu, J.-Z. Song, C. Chen, Q. Zhang, H.-B. Zeng, Y. Luo, and S.-H. Yu, "Ce^{3+}-doping to modulate photoluminescence kinetics for efficient $CsPbBr_3$ nanocrystals based light-emitting diodes," J. Am. Chem. Soc. **140**, 3626 (2018).
[24]A. De, S. Das, N. Mondal, and A. Samanta, "Highly luminescent violet- and blue-emitting stable perovskite nanocrystals," ACS Mater. Lett. **1**, 116 (2019).
[25]S. Li, Z. Shi, F. Zhang, L. Wang, Z. Ma, D. Yang, Z. Yao, D. Wu, T.-T. Xu, Y. Tian, Y. Zhang, C. Shan, and X. J. Li, "Sodium doping-enhanced emission efficiency and stability of $CsPbBr_3$ nanocrystals for white light-emitting devices," Chem. Mater. **31**, 3917 (2019).
[26]Z.-J. Yong, S.-Q. Guo, J.-P. Ma, J.-Y. Zhang, Z.-Y. Li, Y.-M. Chen, B.-B. Zhang, Y. Zhou, J. Shu, J.-L. Gu, L.-R. Zheng, O. M. Bakr, and H.-T. Sun, "Doping-enhanced short-range order of perovskite nanocrystals for near-unity violet luminescence quantum yield," J. Am. Chem. Soc. **140**, 9942 (2018).
[27]N. Mondal, A. De, and A. Samanta, "Achieving near-unity photoluminescence efficiency for blue-violet-emitting perovskite nanocrystals," ACS Energy Lett. **4**, 32 (2019).
[28]S. Seth, T. Ahmed, A. De, and A. Samanta, "Tackling the defects, stability, and photoluminescence of $CsPbX_3$ perovskite nanocrystals," ACS Energy Lett. **4**, 1610–1618 (2019).
[29]V. B. Mykhaylyk, M. Rudko, H. Kraus, V. Kapustianyk, V. Kolomiets, N. Vitoratou, Y. Chornodolskyy, A. S. Voloshinovskiid, and L. Vasylechko, "Ultra-fast low temperature scintillation and X-ray luminescence of $CsPbCl_3$ crystals," J. Mater. Chem. C **11**, 656–665 (2022).
[30]Y. Smortsova, O. Chukova, M. Kirm, V. Nagirnyi, V. Pankratov, A. Kataeva, and A. Kotlov, "The P66 time-resolved VUV spectroscopy beamline at PETRA III storage ring of DESY," J. Synchrotron Radiat. **32**(6), 1539–1548 (2025).
[31]I. P. Pashuk, N. S. Pidzyrajlo, and M. G. Matsko, "Exciton absorption, luminescence and resonance Raman scattering in $CsPbCl_3$ and $CsPbBr_3$ crystals at low temperatures," Fiz. Tverd. Tela **23**(7), 2162–2165 (1981).
[32]K. Nitsch, V. Hamplová, M. Nikl, K. Polák, and M. Rodavá, "Spectroscopic properties of lead halide crystals," Chem. Phys. Lett. **258**, 518–522 (1996).
[33]M. Dendebera, Y. Chornodolskyy, R. Gamernyk, O. Antonyak, I. Pashuk, S. Myagkota, I. Gnilitskyi, V. Pankratov, V. Vistovskyy, V. Mykhaylyk, and M. Grinberg, "Spectroscopic properties of lead halide crystals," J. Lumin. **225**, 117346 (2020).
[34]M. Sebastian, J. A. Peters, C. C. Stoumpos, J. Im, S. S. Kostina, Z. Liu, M. G. Kanatzidis, A. J. Freeman, and B. W. Wessels, "Excitonic emissions and above-band-gap luminescence in the single-crystal perovskite semiconductors $CsPbBr_3$ and $CsPbCl_3$," Phys. Rev. B **92**, 235210 (2015).
[35]J. A. Steele, P. Puech, B. Monserrat, B. Wu, R. X. Yang, T. Kirchartz, H. Yuan, G. Fleury, D. Giovanni, E. Fron, M. Keshavarz, E. Debroye, G. Zhou, T. C. Sum, A. Walsh, J. Hofkens, and M. B. J. Roeffaers, "Thermal unequilibrium of charge carriers in hybrid perovskites," ACS Energy Lett. **4**, 2205–2212 (2019).
[36]W. Du, S. Zhang, Z. Wu, Q. Shang, Y. Mi, J. Chen, C. Qin, X. Qiu, Q. Zhang, and X. Liu, "Enhanced photoluminescence and stability in perovskite nanocrystals through surface ligand engineering," Nanoscale **11**, 3145–3153 (2019).
[37]X. Fang, K. Zhang, Y. Li, L. Yao, Y. Zhang, Y. Wang, W. Zhai, L. Tao, H. Du, and G. Ran, "Effect of excess $PbBr_2$ on photoluminescence spectra of $CH_3NH_3PbBr_3$ perovskite particles at room temperature," Appl. Phys. Lett. **108**, 071109 (2016).
[38]E. M. Hutter, M. C. Gélvez-Rueda, A. Osherov, V. Bulović, F. C. Grozema, S. D. Stranks, and T. J. Savenije, "Direct-indirect character of the bandgap in methylammonium lead iodide perovskite," Nat. Mater. **16**, 115–120 (2017).
[39]F. Pan, J. Li, X. Ma, Y. Nie, B. Liu, and H. Ye, "Free and self-trapped exciton emission in perovskite $CsPbBr_3$ microcrystals," RSC Adv. **12**, 1035 (2022).
[40]C. Wolf and T. W. Lee, "Exciton and lattice dynamics in low-temperature processable $CsPbBr_3$ thin films," Mater. Today Energy **7**, 199–207 (2018).
[41]Z. Liu, Q. Shang, C. Li, L. Zhao, Y. Gao, Q. Li, J. Chen, S. Zhang, X. Liu, Y. Fu, and Q. Zhang, "Temperature-dependent photoluminescence and lasing properties of $CsPbBr_3$ nanowires," Appl. Phys. Lett. **114**, 101902 (2019).
[42]M. Wenzel, M. Altwein, R. Demirbilek, B. Leu, J. Heber, J. Kubler, B. Bleeker, and A. Meijerink, "Band structure and excitons in $CsCdBr_3$," J. Alloys Compd. **300–301**, 479–482 (2000).
[43]K. H. Fausia, B. Nharangatt, R. N. Vinayakan, A. R. Ramesh, V. Santhi, K. R. Dhandapani, T. P. Manoj, R. Chatanathodi, D. Jose, and K. Sandeep, "Probing the structural degradation of $CsPbBr_3$ perovskite nanocrystals in the presence of H_2O and H_2S: How weak interactions and HSAB matter," ACS Omega **9**, 8417–8424 (2024).
[44]P. Ren, J. Qin, and C. Chen, "A novel nonlinear optical crystal for the IR region: Noncentrosymmetrically crystalline $CsCdBr_3$ and its properties," Inorg. Chem. **42**(1), 8–10 (2003).
[45]M. D. Segall, P. J. D. Lindan, M. J. Probert, C. J. Pickard, P. J. Hasnip, S. J. Clark, and M. C. Payne, "First-principles simulation: ideas, illustrations and the CASTEP code," J. Phys.:Condens. Matter **14**, 2717 (2002).
[46]S. M. Loh and S. A. Blundell, "Atomic and electronic properties of doped $CsPbBr_3$ perovskite: An ab initio study," ACS Omega **10**, 53163 (2025).